Engineering Structures 291 (2023) 116462

Contents lists available at ScienceDirect

Engineering Structures

journal homepage: www.elsevier.com/locate/engstruct

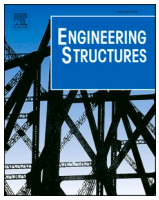

Experimental analysis of the shear resistance of precast concrete T-beams with a top cast-in-place slab

Lisbel Rueda-García [a,*], José L. Bonet [b], Pedro Miguel [b], Miguel Ángel Fernández-Prada [b]

[a] Concrete Science and Technology University Institute (ICITECH), Universitat Politècnica de València, Camí de Vera, no number, 46022, Valencia, Spain
[b] Construction Engineering and Civil Engineering Projects Department and Concrete Science and Technology University Institute (ICITECH), Universitat Politècnica de València, Camí de Vera, no number, 46022, Valencia, Spain

ARTICLE INFO

Keywords:
Precast construction
Reinforced concrete
Composite beam
T-beam
Cast-in-place slab
Shear strength
Shear failure
Interface shear
Mechanical behavior

ABSTRACT

Precast concrete T-beams with a cast-in-place slab on top are structural elements that are often employed in composite construction. Despite their widespread use, some aspects of their structural behaviour upon shear forces have not yet been studied in depth. Six composite specimens with different T-shaped cross-sections and concrete qualities, and with web reinforcement, were tested to analyse the shear transfer mechanisms and to assess the contribution of the cast-in-place slab to shear strength. The shear strength mechanisms deriving from experimental observations and measurements are provided. This study indicates that: placing a concrete cast-in-place slab on top of a prefabricated T-beam increases its shear strength; interface shear strength plays an essential role in concrete composite elements' vertical shear strength; widening the cast-in-place slab width does not increase shear strength in this test programme specimens; the compressive strength of the precast beam's concrete significantly influences composite beams' shear resistances. The ACI 318-19 formulation best captures the influence of concrete strength on shear strength of the three formulations considered (EC2, MC-10 (Level III) and ACI 318-19). However, all of them tend to underestimate shear strengths compared to the experimental results.

1. Introduction

In order to span medium and large distances in the construction of bridges and buildings, the use of precast reinforced or prestressed concrete beams with T- or I-shaped cross-sections is a widespread practice. On top of these beams a cast-in-place concrete layer is poured to enhance the integrity of the overall structure, leading to concrete composite elements. In 2016 the Technical Committee 4.3 "Road bridges" of PIARC revealed that more than 70 % of road bridges in European participating countries are made of reinforced or prestressed concrete [1]. Moreover, the report of PIARC showed that around 60 % of the bridges are more than 40 years old. It is therefore expected that many of the existing bridges will need to be structurally assessed in the short to medium term.

Nowadays, concrete bridges must support increasing loads according to the newest design standards. Moreover, current codes are oriented towards the design of new structures and therefore, subordinate accuracy to ease of use in some respects. Consequently, the current design approaches, when used to evaluate existing structures, may consider them unacceptable, as it is the case of many bridges in service today that show a satisfactory behaviour [2]. For this reason, in the last decade many countries have started developing codes to evaluate existing structures. Given the vast number of concrete composite structures and their age, the detailed study of their structural behaviour is especially important.

In a concrete composite beam, the interface between the two concrete members (usually referred to as "layers") allows relative displacements and transfers coupling forces to the two layers, resulting in systems in partial interaction [3]. The transfer of shear forces at the interface between the two concrete layers is critical for the integrity of composite elements [4,5]. For that reason, the structural analysis of concrete composite beams has traditionally focused on the interface shear strength, which has been well-analysed since the 1960s [6–10].

On vertical shear performance of concrete composite beams, there are fewer experimental studies than on interface shear strength, as Kim *et al.* pointed out in [4,11]. The existing experimental tests on T- or I-shaped concrete beams with top cast-in-place slab study the following shear-related issues. Avendaño and Bayrak [12] analysed in a technical report the horizontal sliding at the bottom flange of prestressed I-shaped concrete girders with a top slab. Nagle and Kuchma in [13] analysed the

* Corresponding author.
E-mail addresses: lisruega@cam.upv.es (L. Rueda-García), jlbonet@cst.upv.es (J.L. Bonet), pmiguel@cst.upv.es (P. Miguel), mafernan@cst.upv.es (M.Á. Fernández-Prada).

https://doi.org/10.1016/j.engstruct.2023.116462
Received 15 July 2022; Received in revised form 21 April 2023; Accepted 8 June 2023

Nomenclature

a	shear span
c	concrete cover
d	effective depth
E_c	concrete's modulus of elasticity
E_s	modulus of elasticity of reinforcement
$f_{c,28}$	compressive strength of the concrete measured in cylinders at the age of 28 days
$f_{c,b}$	compressive strength of the beam's concrete measured in cylinders
$f_{c,wa}$	weighted average of the beam and slab's concrete compressive strengths measured in cylinders estimated from the area ratio
f_{ct}	concrete tensile strength
f_u	tensile strength of reinforcement
f_y	yield strength of reinforcement
f_{yw}	yield strength of transverse reinforcement
h	overall member height
$Ø$	nominal diameter of a reinforcing bar
V	shear force
V_{exp}	experimental shear strength
V_{pred}	specimen's predicted shear strength value
ε_c	strain on the concrete surface
ε_u	reinforcement strain at the maximum load
ε_y	reinforcement strain at yield strength
θ	angle between the strut and the axis of the member
ρ_l	reinforcement ratio of tension longitudinal reinforcement
ρ_w	reinforcement ratio of web reinforcement

application of the shear provisions of AASHTO LRFD Bridge Design Specifications [14] to high-strength concrete members, by testing the shear performance of I-shaped concrete beams with a top slab. In [15], Ross et al. studied how the end region detailing of concrete I-girders with cast-in-place slab affected the shear strength. Ruiz and Muttoni in [16] studied the load-carrying mechanisms of thin-webbed, prestressed beams failing by crushing of the web, which were extracted from an actual bridge. Tawfiq in [17] studied the shear capacity of high-strength concrete girders with a slab on top under fatigue loading. Other publications, such as [18–22], focused on the experimental verification of prestressed concrete girders with cast-in-place slab, which were fabricated on purpose for the tests or salvaged from existing bridges, according to design codes such as AASHTO LRFD [14], previous versions of AASHTO or ACI 318 [23].

In all the studies mentioned above (references [12,13,15–22]), the influence of the presence of an interface in the vertical shear strength of the members was not analysed, which is an issue with little number of research according to Halicka [24]. Furthermore, no analysis about the portion of the shear strength resisted by the slab was made. In a design stage, sometimes the contribution of the slab to the shear resistance is neglected by staying on the side of safety (as indicated in [4]), since shear strength is a phenomenon that still has many unknowns. However, this contribution may be relevant in the assessment of existing structures. Some other times, the effective depth of the whole composite specimen and only the compressive strength of the precast beam concrete are considered in shear strength calculations (for example in [12,19]). This may be reasonable for large girders with a large depth in relation to the depth of the slab but could be unsafe for smaller composite elements, as mentioned in [25], since it is uncertain if the contribution of the high-strength concrete of the precast beam is fully valid in the evaluation of the overall shear strength, as Kim et al. stated in [11]. For all these reasons, it seems necessary to study some questions related to the contribution of the cast-in-place slab to shear strength in concrete composite beams that still need to be analysed in depth, such as which composite element depth, which concrete strength (precast beam concrete or slab concrete) or which slab width must be considered in the shear strength assessment calculations.

Only Halicka and Jabłoński in [24,26] and Kim et al. in [4,11,27,28] carried out experimental tests on concrete composite beams for studying the abovementioned issues. Halicka and Jabłoński's research focused on analysing the effect of the interface on the shear strength by testing rectangular beams and T-beams with the interface between concretes in the plane of cross-section width change. Kim *et al.* tested numerous rectangular composite specimens with and without web reinforcement, made of prestressed and non-prestressed concrete. They mainly analysed the influence on the shear strength of using different concretes at the beam and the slab. However, these authors did not consider the existence of two weak planes (the cross-section width change and the interface between concretes) that T-beams with top slab have, nor other issues such as the slab width that contributes to shear resistance.

Some current design codes have limited indications about the shear capacity of composite elements. For example, Section 10.9.3 of EC2 [29] allows concrete elements with a topping that is at least 40 mm thick to be designed as composite elements, provided that interface shear strength meets code requirements. However, no further indications are given about how these composite elements must be designed. Section 22.5.4 of ACI 318-19 [23] also indicates that the interface must be designed for the loads that will be transferred across it, and specifies that shear strength may be calculated with the properties of the element (precast beam or slab) that result in the most critical value or the properties of the individual elements. Nevertheless, further experimental evidence is required for verifying the result of individual elements because the current ACI 318 design equation was developed based on test results obtained with monolithic beams [4]. The PCI Bridge Design Manual [30] considers the effective depth of the composite section in its design examples of bridge girders with the AASHTO LRFD Specifications [14], but the general procedure still considers the precast beam concrete strength, not yet solving the problem stated by Kim *et al.* in [4,11] about the effect of dual concrete strengths. Other current codes, such as MC-10 [31], do not mention this type of structural elements.

As a preliminary step to the shear study of T-beams with top cast-in-place slab, the authors analysed in previous publications [32–34] the shear strength of simpler specimens with a delimited number of parameters. Monolithic and composite rectangular and T-shaped beams both with and without shear reinforcement, whose main characteristics and results are later described in Section 2 of this paper, were tested under shear forces. The main findings from these studies were:

1. Both the interface between concretes and the plane on which section width changes in monolithic T-shaped specimens were a weakness plane that clearly modified the crack pattern of specimens by deviating the diagonal shear cracks along it.
2. The horizontal crack along that weakness plane divided shear transmission into two load paths: one through the precast beam web and one through the beam head or cast-in-place slab.
3. Specimens' failure was given by the failure of the shear path through the beam head or the slab.

All these findings were captured in a formulation based on a strut-and-tie model proposed by the authors for assessing the shear strengths of the specimens.

Given that both the interface and section width change can modify the crack pattern and, thus, the shear strength mechanisms of

specimens, the aim of this paper is to study the contribution of the cast-in-place slab to shear strength in structures that have both weakness planes, such as T-beams with a cast-in-place slab on top, because they have been frequently used in precast constructions since long ago, as explained above. For this purpose, six T-shaped specimens were experimentally tested. They were made of reinforced concrete with shear reinforcement, a high longitudinal reinforcement ratio and subjected to shear forces. The specimens were designed so that the interface between concretes would influence their crack patterns and, thus, their shear strength mechanisms. A pure horizontal shear failure of the specimens and a monolithic behaviour (i.e., cracks cross the interface without developing horizontally along it, so the composite specimen behaves as monolithic), which have already been studied in multiple publications, were avoided. The following items that influence shear strength were analysed by comparing different cross-section types and concrete qualities:

- The presence of a cast-in-place slab on top.
- The presence of an interface between concretes.
- The cast-in-place slab width.
- The compressive strength of the beam and slab concretes.

The results of this analysis are herein presented. The experimental results are also compared to the shear strength predictions of current codes' shear formulations.

The research significance of this paper lies in it providing novel experimental results of concrete composite beams formed by a T-beam and a top slab for analysing shear-strength related-aspects, which have been little studied in the literature, such as the influence of an interface between concretes in vertical shear strength and the contribution of the cast-in-place slab to shear strength. Predicting this contribution is an open issue that designers face in practice and one that still needs to be solved, mainly on the accurate assessment of existing structures. The tests performed in this paper provide primary results for the future analysis of more complex elements commonly used in practice, such as prestressed members. The study herein performed of shear strength mechanisms sheds light on these structures' shear behaviour and provides the basis for future development of a shear design and assessment formulation for composite concrete elements. Moreover, the experimental results presented in this study could be used in the adjustment of future numerical models that represent the behaviour of concrete composite beams.

The paper structure consists of a brief description of the previous experimental tests performed by the authors, a detailed explanation of the tests carried out in this research and the test results, an analysis of the failure modes and the effect of the test parameters on shear strength, a comparison of the test results with existing code provisions and a list of the conclusions derived from this research.

2. Previous experimental tests carried out by the authors

The main objective of this research project is to experimentally analyse the shear strength of concrete composite beams with web reinforcement, commonly used in bridge decks (see the example of Fig. 1). Given the multiple variables that can affect their behaviour, some preliminary experimental tests were carried out by the authors in previous publications [32–34], in which simpler specimens with a delimited number of parameters were analysed in shear.

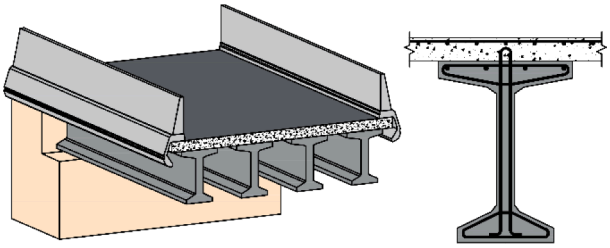

Fig. 1. Example of bridge deck made of concrete composite beams.

These preliminary tests consisted of simply supported beams with two point loads on top that had different cross-sectional shapes (see Fig. 2). The specimens with cross-section type A1 were fabricated to study the shear strength of only the precast beam and compare it to the shear strength of a specimen with a cast-in-place slab on top (B2). The B1 specimens were made to analyse the influence of an interface between concretes on shear strength, by comparing them to B2 specimens. The influence of the flanges of a T-beam on shear strength was studied by means of C1 and D1 specimens. In previous studies [35], wider flanges than once the flange depth (C1 specimens) are considered to not increase shear strength. Moreover, some shear strength approaches about the shear-effective area of the compression chord in T-beams consider that the area increases by approx. 45° from the cross-section width change [36]. These statements were verified by comparing C1 and D1 specimens. Finally, the influence of an interface between concretes in T-shaped beams was studied by fabricating C2 and D2 specimens and comparing them to C1 and D1 specimens, respectively. Other parameters that influence the shear strength were studied, such as the shear reinforcement ratio ρ_w (specimens had $\rho_w = 0$ or $\rho_w = 0.22$ %), the concrete compressive strength of the precast beam ($f_{c,b}$) and the differential shrinkage between concretes.

In order to make all the specimens comparable between them, some parameters were fixed:

- The longitudinal reinforcement ratio ($\rho_l = 4.0$ %). Since the shear strength increase provided by the flanges in T-shaped beams is uncertain, a high ρ_l was chosen to avoid bending failure prior to shear failure in all the specimens of the experimental programme.
- The shear span-effective depth ratio ($a/d = 4.0$). The specimens were designed to foster a shear failure mainly governed by beam shear-transfer actions (cantilever action, aggregate interlock, dowel action and residual tensile strength of concrete, as defined in [37]) in both rectangular specimens and T-shaped specimens and to avoid an overstrength due to the arching action (left side of the well-known "Kani's valley" [37,38]).
- Relative concrete cover ($c/h = 0.16$). The concrete cover may affect the shear behaviour of the specimens, so it was fixed to ensure that it has no influence.
- The yield strength of the web reinforcement steel ($f_{yw} = 538$ MPa). The same steel was used in all the stirrups to ensure shear strength does not depend on f_{yw}.

Multiple results were obtained from these preliminary tests in relation to the variables studied. The main results to be considered in the tests of the present research work were those related to the cracking of the specimens and their failure modes.

The most known shear failure modes in monolithic reinforced concrete beams with shear reinforcement are, as explained in [39], (i) the failure of the diagonal compression struts (crushing of the web), typical of thin-webbed precast beams; (ii) the failure of the compression chord; (iii) the tension failure at the web (or failure of the stirrups); (iv) the shear failure initiated by failure of the tension chord due to insufficient longitudinal reinforcement. In the monolithic rectangular specimens of this test programme the failure was given by the compression chord long after the stirrups yielded (see Fig. 3a), as described in [33].

In the composite specimens, as shown in Fig. 3, the interface between concretes modified the crack pattern (Fig. 3b,d) in comparison to that of a monolithic rectangular specimen (Fig. 3a). The interface forced the diagonal shear cracks to develop horizontally along it. A similar effect had the cross-section width change in T-beams (Fig. 3c).

These differences in the crack patterns of the specimens had a big influence on the transmission of the shear force to the supports. The

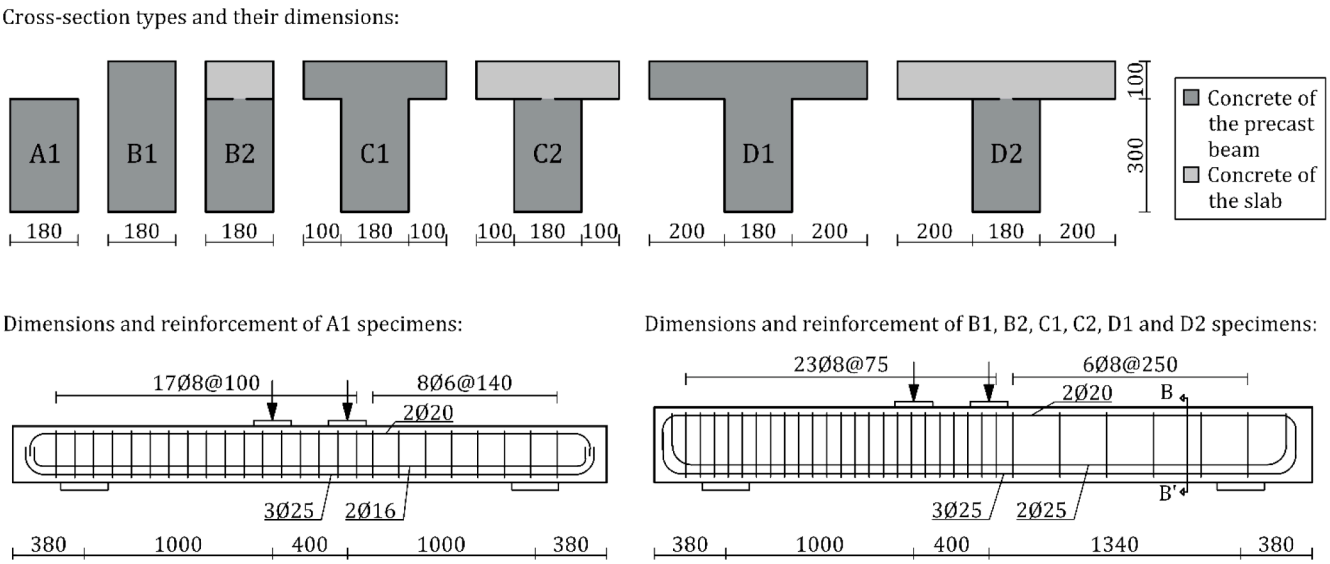

Fig. 2. Cross-section types, dimensions and reinforcement of the specimens of the previous tests carried out by the authors [32–34] (dimensions: mm).

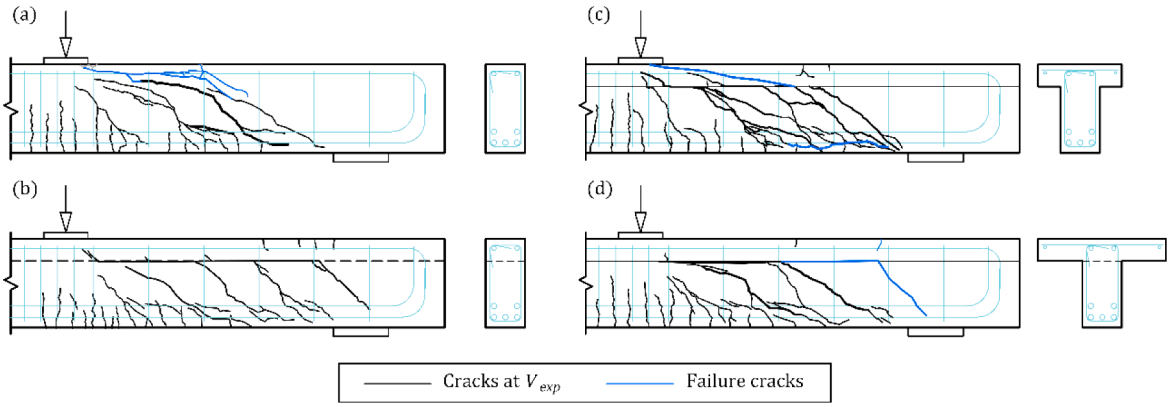

Fig. 3. Examples of crack patterns: (a) monolithic rectangular beam (NWP2B1 in [33]); (b) composite rectangular beam (NWP3B2 in [33]); (c) monolithic T-beam (NWP2C1 in [34]); (d) composite T-shaped beam (NWP2D2 in [34]).

horizontal crack along the weakness plane (interface or the cross-section width change) divided the transmission of the shear force into two paths: one through the web below the weakness plane and one through the slab or flanges above the weakness plane. The authors observed the shear force at the lower path was mainly resisted by the web reinforcement, while the upper path behaved as a concrete member without shear reinforcement [33]. Both shear paths were connected at the weakness plane crack by means of the dowel action of the web reinforcement crossing the interface and the aggregate interlock action along the crack.

The failure of the specimens was given by the failure of the upper shear transmission path. Three failure modes were observed in the specimens tested with a concrete-to-concrete interface or a cross-section width change [34]:

- Slab bending failure (BF). The formation of bending cracks on top of the specimens near the supports and the gradual drop of the shear-deflection curve indicated the bending failure of the upper path (Fig. 3b).
- Slab shear failure (SF). The formation of a sudden diagonal crack at the upper path and a marked load drop pointed out the shear failure of the slab (Fig. 3c).
- Interface failure (IF). The sudden development of the horizontal crack in direction to the support and a marked load drop indicated the failure of the interface (Fig. 3d).

Even though the interface between concretes modified the shear strength mechanisms, the composite rectangular specimens with similar concrete compressive strength in both the beam and the slab showed similar shear strength values to those of monolithic rectangular specimens. On the contrary, in T-shaped specimens the presence of an interface between concretes at the height of the cross-section width change decreased their shear strengths in comparison to those of monolithic T-beams, since the interface usually led to weaker shear failure mechanisms, such as BF, which do not allow the flanges to contribute to shear strength as they do in SF [34].

Finally, in the T-shaped specimens with SF, it was experimentally obtained that the flanges increased shear strength in the same proportion as the shear-effective area increases when an effective slab width equal to the web width and once the flange depth is considered (approx. 17 %) [34].

3. Materials and methods

3.1. Test parameters

The variable parameters considered in the specimens of this study to analyse the cast-in-place slab's contribution to shear strength were the following:

- Presence of a cast-in-place slab on top. Specimens E2 (see Fig. 4), formed by a monolithic T-beam (representing the precast beam) with a cast-in-place slab on top, were fabricated to be compared to specimens C1 from the previous experimental study by the authors [34] (see Fig. 2). Specimens C1 had the same characteristics and dimensions as the monolithic T-beam of specimen E2, but without any cast-in-place slab on top.
- Presence of an interface between concretes. Specimens E1 (see Fig. 4) were monolithically fabricated. Specimens E2 were fabricated with two concretes cast at different times, so an interface between both concretes was created.
- Slab width. Two different slab widths were designed to be compared in this study. First, that of specimen E2, whose slab width equalled the flange width of the monolithic T-beam. Second, that of specimen F2, more similar to the target geometry of the example of Fig. 1, whose slab was wider than the flange of the monolithic T-beam (see Fig. 4) to verify if the shear-effective area of the slab also increases by approx. 45° from the interface, as considered in some approaches for monolithic T-beams [36].
- Beam and slab concretes' compressive strengths. Two different compressive strengths for the precast beam concretes were used: normal-strength concrete (NSC), whose design compressive strength was 25 MPa; high-strength concrete (HSC), whose design compressive strength was 70 MPa. All the cast-in-place slabs were designed with NSC.

3.2. Test specimens

Six specimens were tested in this experimental programme. Table 1 summarises their main characteristics. Two series of three reinforced concrete T-shaped specimens with web reinforcement were fabricated. In the first series (series NW), the three specimens (one for each cross-section type; E1, E2 and F2 in Fig. 4), were fabricated with normal-strength concrete (NSC) at both the precast beam and the cast-in-place slab. In the second series (series HW), the entire beam in specimen E1 and the precast beams of the composite specimens were fabricated with high-strength concrete (HSC); the slabs were produced with NSC.

None of the specimens of this article was replicated. Thus, the validity of the experimental results was based on the adequate deviations of the shear strengths observed in the replication of the previous experimental tests of the experimental programme, whose design was similar to that of these specimens, as shown in Section 2, and were published in [32–34]. The coefficient of variation (CV) of the shear strengths was 6 % on average for all the replicated specimens (13 different beam types out of 29 beam types were replicated between two and five times).

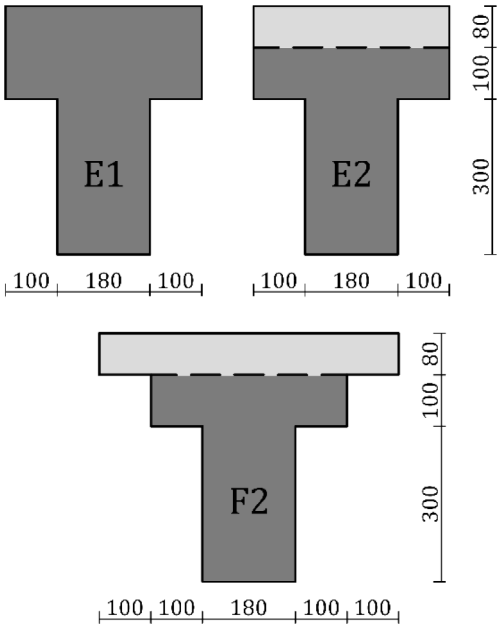

Fig. 4. Cross-section types (dimensions: mm).

The nomenclature of the six specimens was as follows: *xWzk*, where "*xW*" referred to the series name (NW or HW as explained above), "*z*" represented the cross-section shape (E or F in Fig. 4), and "*k*" denoted the number of concretes used to fabricate the specimen (1 for monolithic specimens, 2 for composite specimens).

Fig. 5 shows the dimensions and reinforcement of the specimens for each cross-section type. Specimens were 4.14 m long. The distance between supports was 3.00 m. Two non-centred point loads, separated by 0.40 m, applied the load to the top of beams and formed two different shear spans: a 1.60 m-long principal span where failure was expected; a 1.00 m-long reinforced span with additional web reinforcement to prevent shear failure. All the specimens were 0.48 m high (see Fig. 4). In the composite specimens (E2 and F2), the precast beam was 0.40 m high and the cast-in-place slab was 0.08 m high.

These specimens had fixed the same parameters as the specimens from the previous series (see Section 2) to make them comparable to each other: $a/d = 4$, which was selected to foster a shear failure governed by beam shear-transfer actions and not affected by an overstrength due to the arching action (see [37]); $\rho_l = 4.3$ %, to prevent bending failure in all the specimens, including those with the widest flanges; $c/h = 0.16$; $f_{yw} = 538$ MPa. Moreover, the 6 specimens had shear reinforcement, so ρ_w was fixed to 0.22 %, which met the most restrictive maximum spacing requirement of all the current codes considered in the design of these beams [23,29,31] to minimise the reinforcement. The interface roughness in all the composite specimens was "smooth" or "as-cast" according to current code definitions as concrete underwent no further treatment after vibration.

The interface reinforcement ratio, which equalled the shear reinforcement ratio (0.22 %), and interface roughness were selected after a previous work by the authors [40] proved that they were appropriate for ensuring diagonal beam cracking before interface cracking. The transverse reinforcement at the flange of the T-beams and at the slab was designed to prevent the shear failure between web and flanges in both. Finally in the composite specimens, the time that elapsed between the precast beam concrete casting and the slab concrete casting was 24 h, which was set after a previous study by the authors [33] proved that marked differential shrinkage between the precast beam and slab concretes did not significantly influence the shear strength of the specimens of this experimental programme.

3.3. Fabrication of specimens

The fabrication process of the two specimen series (NW and HW) was conducted on two consecutive days. The precast beam concrete was poured on the first day. In the composite specimens, the concrete surface of the principal span, where failure was expected, was not further treated after vibration. Thus interface roughness was "smooth" or "as-cast". In the reinforced span, the surface was racked before concrete hardened to increase the interface shear strength in that span. "Very rough" interface roughness was obtained in that way. The slab concrete was poured in the composite specimens on the second day.

In this experimental programme, the precast beam concrete and the slab concrete were both cast while the entire length of beams was laid on the floor. Hence the beam and the slab of the composite specimens were simultaneously loaded.

3.4. Material properties

Table 2 shows the mechanical properties of the precast beam and slab concretes: the 28-day compressive strength ($f_{c,28}$), and the

Table 1
Main characteristics of the test specimens and their shear strength results.

Specimen	Type of precast beam concrete	Type of slab concrete	T-beam flange width (mm)	T-beam flange depth (mm)	Slab width (mm)	Slab depth (mm)	V_{exp} (kN)
NWE1	NSC	NSC	380	180	–	–	259
NWE2	NSC	NSC	380	100	380	80	241
NWF2	NSC	NSC	380	100	580	80	223
HWE1	HSC	NSC	380	180	–	–	327
HWE2	HSC	NSC	380	100	380	80	315
HWF2	HSC	NSC	380	100	580	80	315

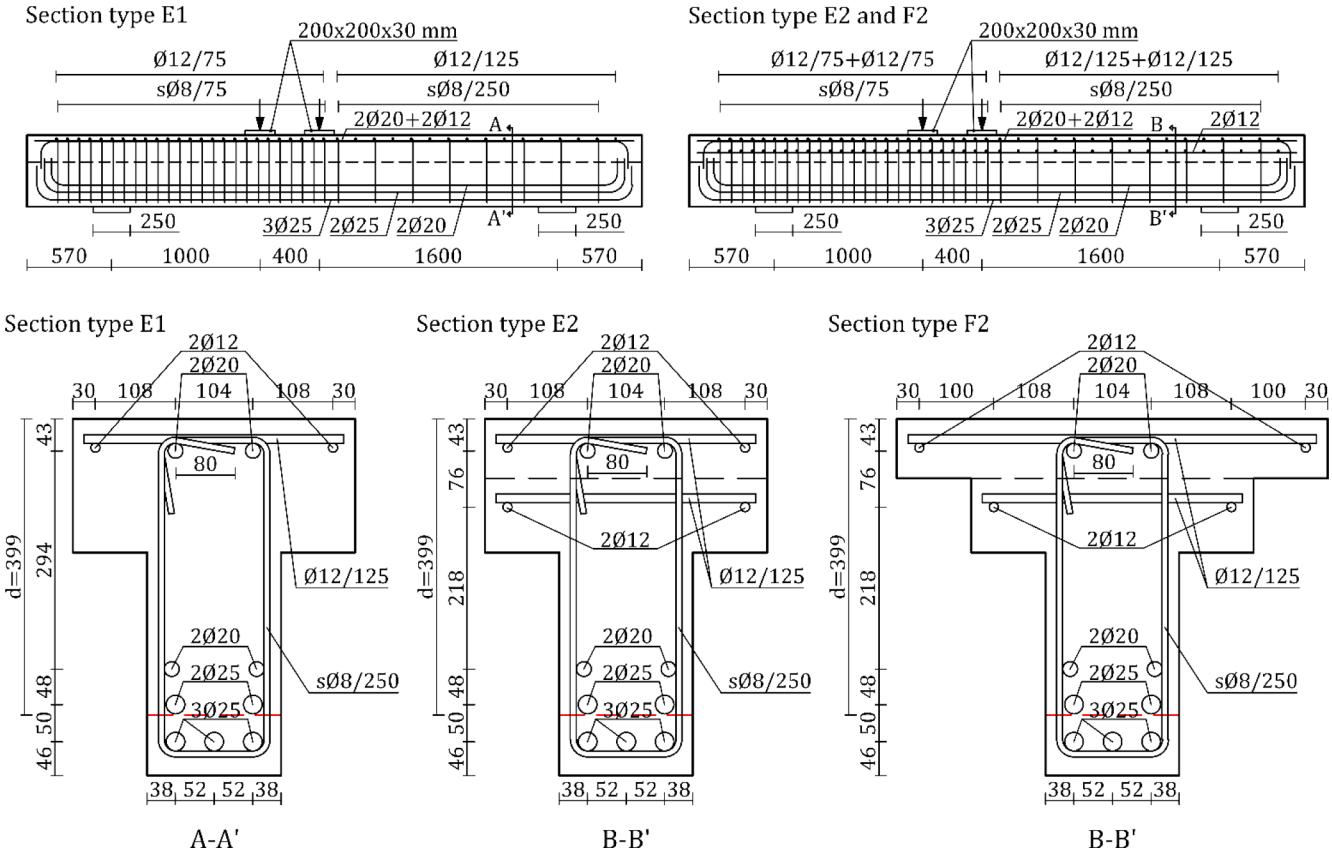

Fig. 5. Dimensions and reinforcement of the specimens with cross-section type E and F (dimensions: mm).

Table 2
Concrete mechanical properties.

Series	$f_{c,28,b}$ (MPa)	$f_{c,28,s}$ (MPa)	$f_{c,b}$ (MPa)	$f_{c,s}$ (MPa)	$E_{c,b}$ (MPa)	$E_{c,s}$ (MPa)	$f_{ct,b}$ (MPa)	$f_{ct,s}$ (MPa)
NW	25	26	25	26	22,386	23,716	1.93	2.18
HW	63	29	67	30	33,438	26,288	4.06	2.69

Notation: suffix "b" refers to the beam's concrete; suffix "s" refers to the slab's concrete.
Average coefficients of variation of measurements: 2 % for $f_{c,28}$ and f_c; 4 % for E_c; 5 % for f_{ct}.

compressive strength (f_c), modulus of elasticity (E_c) and tensile strength (f_{ct}) at testing age. Specimens of series NW and HW were respectively tested 29 and 33 days after precast beam concrete pouring. The results were the average of two concrete cylinders (300 mm high, 150 mm diameter), and were obtained by following the provisions of UNE-EN 12,390 [41–43]. Concrete tensile strength was calculated as 90 % concrete tensile splitting strength, as indicated in [44]. Table 2 shows the average coefficients of variation (CV) of the measurements.

NSC had a water-cement ratio of 0.52, 325 kg/m^3 of Portland cement and a maximum aggregate size of 10 mm. Conversely HSC had 0.44, 500 kg/m^3 and 10 mm.

The reinforcing steel mechanical properties are shown in Table 3.

Table 3
Average values of the transverse and longitudinal reinforcement properties.

Ø (mm)	f_y (MPa)	E_s (GPa)	ε_y (%)	f_u (MPa)	ε_u (%)
8[1]	538	203	0.26	658	12.0
8[2]	515	218	0.24	647	36.4
12	529	196	0.27	651	30.3
20	541	194	0.28	654	26.7
25	548	235	0.23	658	21.6

[1] Stirrups of the principal span.
[2] Stirrups of the reinforced span.

They were measured according to UNE-EN ISO 6892 [45] by averaging the results of two tests for each nominal diameter. Type C steel was used in these specimens according to EC2 [29].

3.5. Instrumentation

The strains on the surface of the reinforcing steel bars were measured by strain gauges (2 mm measuring length, 120 Ω resistance). Their locations are shown in Fig. 6a. Three pairs of strain gauges were located on the bottom bars of the tension longitudinal reinforcement on Sections A to C (see gauges G1 to G6 in Fig. 6a-b). A pair of strain gauges was located at the compression longitudinal reinforcement on Section C (G7 and G8). Five pairs of strain gauges were glued at the mid-length of the two legs of stirrups w4 to w8 (G9 to G18 in Fig. 6a).

The strains on the concrete surface were measured on top of specimens by strain gauges (60 mm measuring length, 120 Ω resistance). Three strain gauges were placed on Sections A and B (gauges C1 to C6 in Fig. 6a). Their locations for beam types E and F are shown in Fig. 6b.

Linear variable displacement transformers (LVDTs) were used at different locations: V1 to V5 (see Fig. 6c), to measure the vertical displacements on the concrete surface; O1 and O2, fixed at the top and bottom of the specimens to detect the beginning of cracking; horizontally placed LVDTs to measure the horizontal slip between the web and flanges (H1 to H4 in Fig. 6c) and between flanges and the slab (H5 to H8 in Fig. 6c). In specimens E1 (see Fig. 4), built monolithically without a slab, LVDTs H5 to H8 were not placed.

The forces at the hydraulic jack and the two bearing points were measured by three 1,000 kN load cells.

Three digital cameras took pictures during the tests at a rate of 0.5 Hz. They were synchronised with the measured load to assign each photogram to the corresponding load. A high-speed camera taking 1000 frames per second was used to detect the beginning of cracking and to record brittle failures.

3.6. Test setup and procedure

A 1,200 kN hydraulic jack, fixed to a steel loading frame placed transversely to the beam's axis (see Fig. 7), applied the vertical load with displacement control (0.02 mm/s). A steel frame, equipped with a hinge to keep the load vertical despite the different displacement of the beam's upper plane, divided the load into two equal point loads. These two loads were transmitted to the specimen by means of two square steel plates (200 × 200 × 30 mm), which were centred on the beam's upper plane width. Beams were laid on two bearing points that consisted of a steel plate (250 mm width), a steel box with steel balls inside (as in [46]) to release horizontal reactions and a hinge to allow for rotations. This same bearing point system was used and explained in the previous

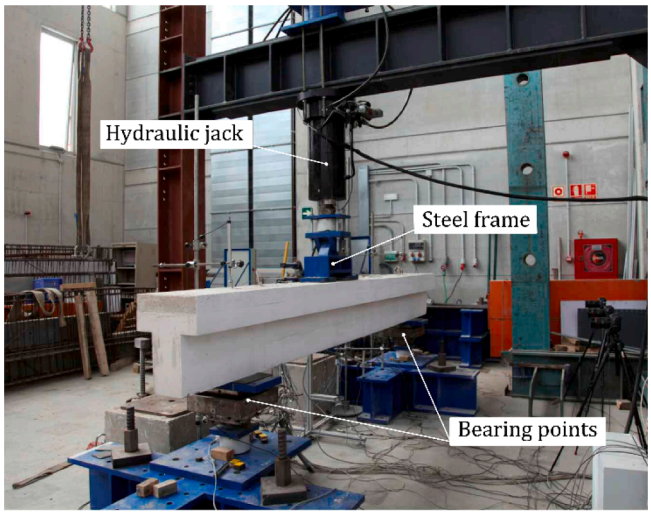

Fig. 7. Experimental setup.

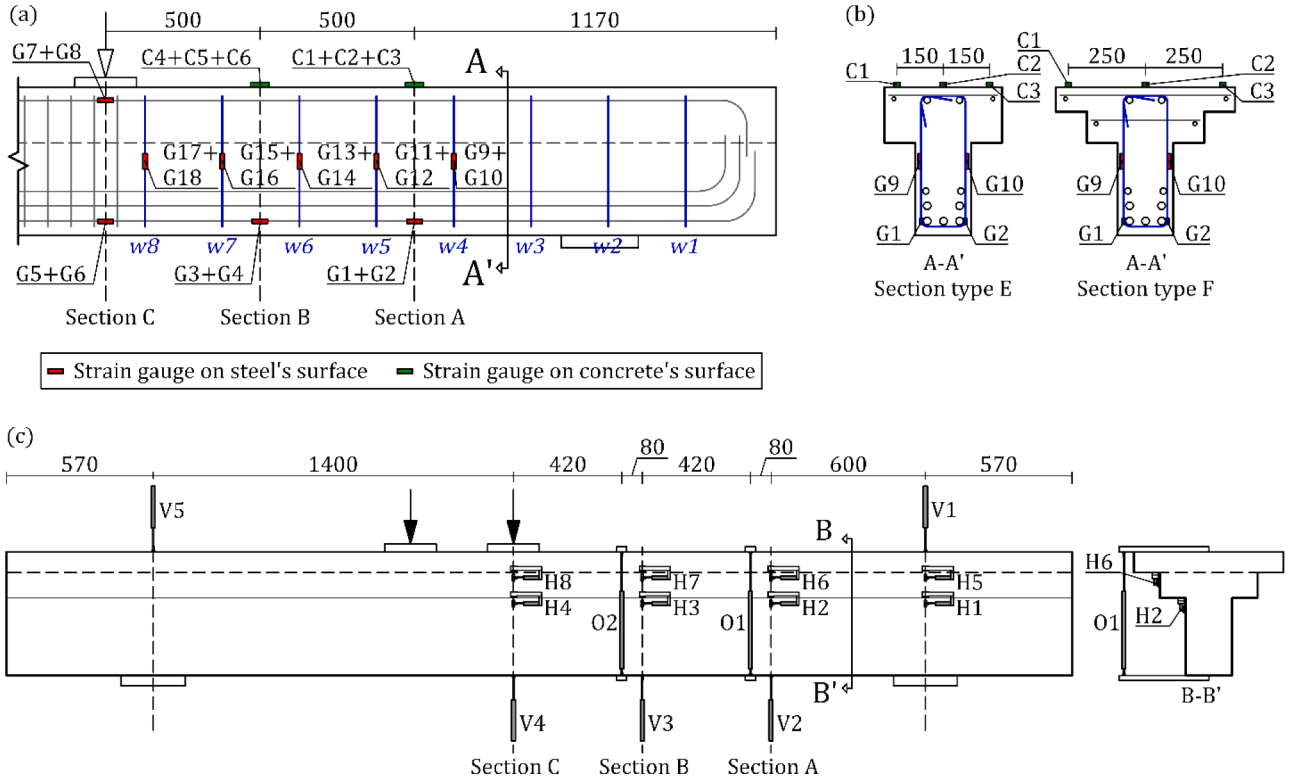

Fig. 6. Instrumentation of the tests: (a) strain gauges at the principal span; (b) strain gauges at section A-A' for beam types E and F; (c) LVDTs (dimensions: mm).

publications by the authors and the research team [32,33,47].

4. Test results

4.1. Shear strength and shear-deflection relation

Specimens' vertical shear strengths are shown in Table 1 as V_{exp}. The relationship throughout the test between shear force V at the principal span and the deflection below the point load (measured by LVDT V4, located on Section C in Fig. 6c) is shown in Fig. 8 for all the test specimens. The maximum shear force (V_{exp}) is marked with a solid circle on each curve.

4.2. Crack patterns

The crack patterns of the test specimens at different load stages, which were drawn using the photographs that the digital cameras took throughout the tests, are shown in Fig. 9. The cracks observed at the maximum shear force V_{exp} are coloured in black. The failure cracks, which are those cracks that appeared immediately after the test reached V_{exp} (observed in the photograph following that of the maximum load), are coloured in blue. The failure cracks were normally accompanied by a load drop (see the shear-deflection curves in Fig. 8) and caused the failure of the specimen. In some specimens the load gradually descended after V_{exp} (see NWE2 and NWF2 in Fig. 8), so the test was stopped when a load loss of around 40 % of the maximum load was reached. The cracks that appeared until the end of the test are coloured in purple.

All the specimens showed similar crack patterns in the first load stages (see Fig. 10a,b about the crack progression for specimens HWE1 and NWF2). Vertical bending cracks appeared for low load levels with a spacing of approx. 80 mm. With increasing load, the bending cracks located below the point loads developed vertically, while the bending cracks located at the shear span changed their trajectory in the direction of the point load, which is frequently observed in shear tests [26,48], and formed diagonal shear cracks. These diagonal cracks had a similar inclination for all the specimens (around 30° to the beam axis), which was also similar to that observed in the monolithic T-shaped specimens with the cross-section type C1 of [34] (see Fig. 3c).

When the diagonal cracks of the principal span reached the plane in which section width changes (flange-web intersection), they developed along that plane before penetrating the beam flange in the direction of the point load (see Fig. 10c,d). This crack pattern has often been described in T-beams in the literature [2,35,48–51]. It was observed in all the specimens of this test programme since their lower part was a T-beam.

In the monolithic specimens (NWE1 and HWE1 in Fig. 9), the crack pattern upon the maximum shear load showed how these diagonal cracks penetrated the beam flange. The diagonal cracks of these beams showed crack widths of around 1–2 mm at V_{exp}. In these specimens, sudden diagonal cracks crossed the flange immediately after V_{exp} (see Fig. 9 and Fig. 10e) with a pronounced load drop, as observed in the shear-deflection curves in Fig. 8a. These specimens' crack pattern was similar to that of the specimens C1 of [34] (Fig. 3c).

In the composite specimens (both E2 and F2), the diagonal cracks that penetrated the beam flange after surpassing the flange-web intersection stopped developing diagonally when they reached the interface plane between concretes (see Fig. 10d). The cast-in-place slab remained intact until V_{exp} because the diagonal cracks did not continue over the interface. At V_{exp}, the crack widths of diagonal cracks were around 1–2 mm for specimens NWE2, HWE2 and HWF2 and around 0.5 mm for specimen NWF2. In all the composite specimens, an interface crack developed in this plane before reaching V_{exp} or immediately afterwards (see Fig. 9 and Fig. 10f). This interface crack has been observed in many composite specimens tested by the authors in previous studies [33,34] (see the example of Fig. 3d). In specimen NWE2, a crack at the interface between concretes appeared shortly before the maximum shear load was reached (Fig. 9) at a load of around 235 kN (V_{exp} was 241 kN; see Table 1), with no noticeable load drop. In specimen NWF2, this interface crack suddenly developed after reaching V_{exp}, and was accompanied by a slight load drop (see Fig. 8c). In specimen HWE2 an extended interface crack appeared immediately after V_{exp} with a pronounced load drop (see Fig. 8b). Specimen HWF2 showed an interface crack that developed horizontally along the flange of the T-beam approximately at the height of the flange transverse reinforcement (see Fig. 5), also with a pronounced load drop (Fig. 8c).

In all the specimens, vertical cracks appeared on top of the slab (see Fig. 9), mainly in the area located over the point at which the diagonal cracks closer to the support reached the flange-web intersection.

4.3. Experimental measurements

This section presents the most relevant results from the instrumentation.

First of all, the measurements of the strain gauges located at the mid-length of stirrups w4 to w8 (see Fig. 6a) at V_{exp} were analysed. The strain of stirrups w4 to w7 reached the steel yield strain in tension in all the

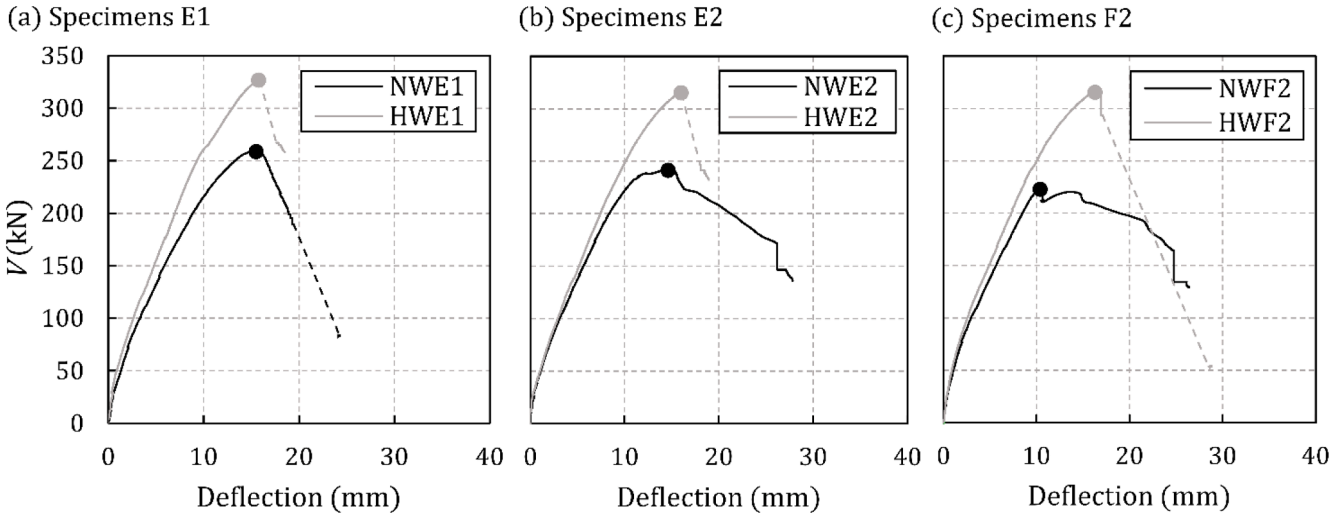

Fig. 8. Shear-deflection relation of the test specimens: (a) specimens with cross-section type E1; (b) specimens with cross-section type E2; (c) specimens with cross-section type F2.

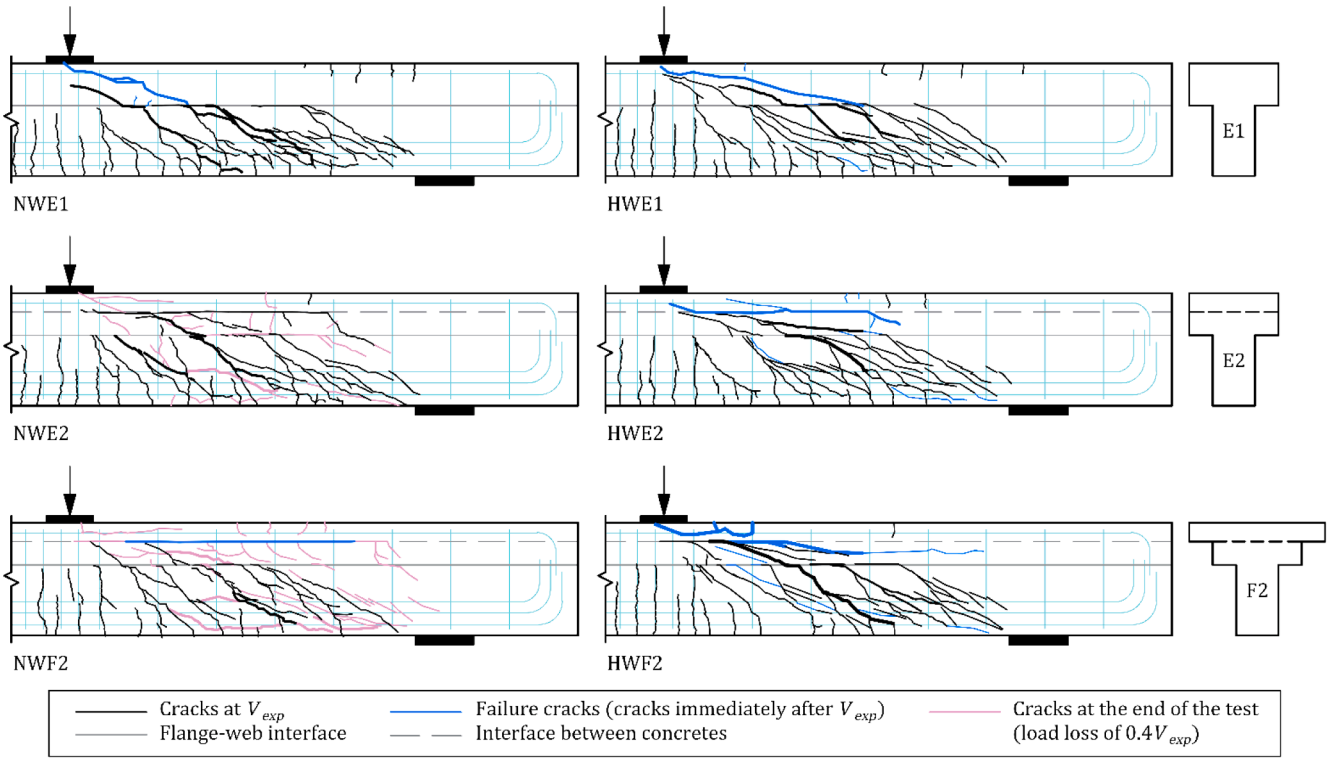

Fig. 9. Crack patterns of the test specimens at different test stages.

specimens, which was 0.26 % (see Table 3). The pair of gauges located at stirrup w8 gave lower strains in tension and were 0.17 % on average for all the tested specimens.

The average strains measured at V_{exp} by the pair of strain gauges located on the tension longitudinal reinforcement at Section C (gauges G5 and G6 in Fig. 6a) below the point load were also analysed. In the series NW specimens, gauges measured a lower average strain than the steel yield strain in tension (0.23 % according to Table 3), which was 0.21 % on average for the three specimens. In the series HW specimens, the tension strains measured at V_{exp} were slightly higher than the yield strain, with 0.26 % on average for all three specimens.

Finally, the strains measured throughout the tests by the strain gauges located on top of specimens (C1 to C3 at Section A and C4 to C6 at Section B, as shown in Fig. 6a) are presented in Fig. 11.

5. Mechanical behaviour and failure modes

5.1. Monolithic specimens

Both monolithic specimens NWE1 and HWE1 showed similar crack patterns. Before V_{exp}, diagonal cracks reached the flange-web intersection and developed horizontally along this weakness plane before entering the flange. Immediately after V_{exp}, one diagonal crack suddenly crossed the flange towards the point load and caused specimen failure. This behaviour was similar to that observed in monolithic T-shaped specimens with less slab depth such as those previously tested by the authors (specimens C1 in Section 2) and those from other authors such as Leonhardt & Walther or Placas [35,51]. Thus the proposal of the authors about the shear strength mechanism of specimens C1 based on the experimental observations and published in [34] is adapted herein to explain the failure mode of the specimens in this paper.

The flange-web intersection crack divided the transmission of shear into two load paths: one through the web below the flange-web intersection and one through the flange (both these load paths are represented in Fig. 12 by means of a strut-and-tie model). At the beam web, shear was transmitted by means of a multiple truss, in which vertical ties were the specimen's stirrups. At the flange a single truss was used, which represented the shear transmission at the beam head of a member without shear reinforcement. Both shear paths were connected at the flange-web intersection crack nodes, where the dowel forces of stirrups and the aggregate interlock action at the interface crack were considered to act.

As observed in previous research works by the authors [33,34], the maximum shear load transmitted by the web shear path was considered to be limited by the yielding of the stirrups and the inclination of the compression field struts at the web. Thus the shear transmitted through this path remained constant for higher loads, and the specimen's shear strength was reached upon the beam head's failure. As a diagonal crack suddenly crossed the flange immediately after V_{exp} (see Fig. 9), the beam head in the monolithic specimens was considered to fail in shear. So the failure mode of specimens E1 was identified as "slab shear failure" (SF).

The explained shear strength mechanism was supported not only by the above-described crack pattern characteristics but also by the following experimental measurements. As indicated in Section 4.3, the measurements of the strain gauges located on the stirrups of the principal span (w4 to w7 in Fig. 6a) showed they reached the steel yielding strain. Furthermore, the strains measured at concrete surface in Section A (gauges C1–C3 in Fig. 11) showed a clear tendency towards tension, which is consistent with the tension tie of the flange strut-and-tie model in Fig. 12. The strain measured by the gauges located at Section B (C4–C6) slightly changed from compression towards tension about halfway through the test. This is also consistent with the section being close to a transition area between compression and tension according to the strut-and-tie model in Fig. 12. Finally, vertical cracks on top of the flange appeared in the tension area, as observed in Fig. 9 and Fig. 12, which verified the existence of tension stresses.

Based on the above description of the mechanical behaviour and the failure modes of the specimens, the shear strength can be considered as the addition of two main components corresponding to the shear capacity of the web and the flange:

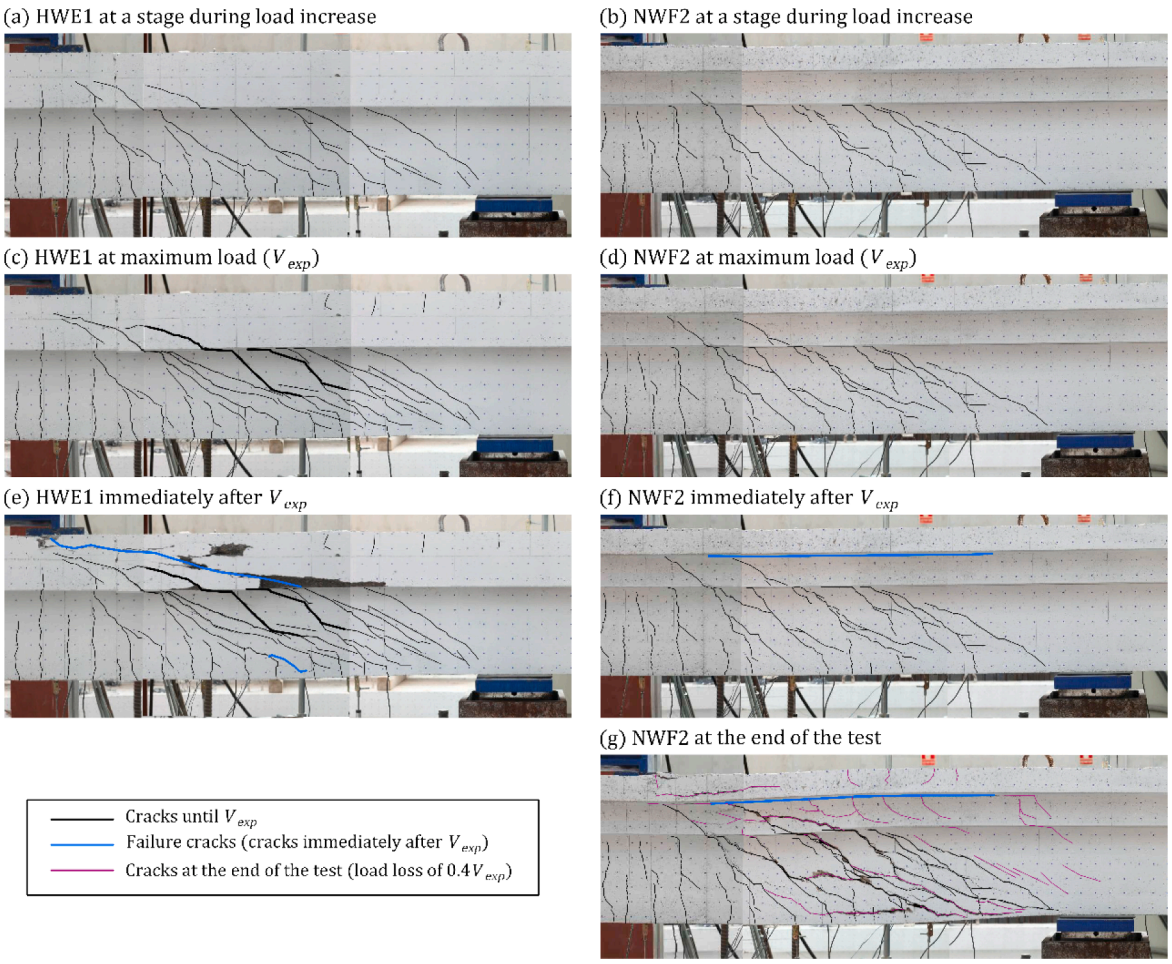

Fig. 10. Examples of crack progression of the monolithic specimen HWE1 and the composite specimen NWF2 at different load stages: (a and b) at a stage during load increase; (c and d) at V_{exp}; (e and f) immediately after V_{exp}; (g) at a load loss of $0.4V_{exp}$.

a) The contribution to the strength of the web is given by the yielding of the stirrups and the inclination of the compression field. Since large cracks develop in the web, an energetic size effect is expected to be dominant over a statistical size effect in this path. Notwithstanding, according to the findings of Yu and Bažant [52], the presence of stirrups would mitigate the size effect on the contribution of the web to the shear strength for small-size specimens (up to 1 m beam depth), such as those of this experimental programme. Therefore, the influence of the size effect on the contribution of the web to the shear strength might be of little relevance in small-size specimens, but not negligible, and should be considered if a concrete contribution is taken into account in its formulation.

b) The flange is assumed to be a member without shear reinforcement and, as observed, fails suddenly by growing a diagonal crack that crosses the flange that develops from a web crack. Therefore, this shear strength component could be affected by a deterministic size effect. Moreover, the observed fragile nature of this failure leads to thinking that this shear strength contribution is highly dependent on size. Therefore, the size effect should be considered in formulating this shear strength contribution. One way to consider the size effect in future mechanical models would be by using the fracture mechanics size effect law proposed by Bažant and Yu [53,54] and adopted by ACI Committee 446, Fracture Mechanics [55]. Further experimental tests on specimens with different flange heights should be carried out to calibrate the suitable brittleness number for this kind of structure [56]. Furthermore, a statistical size effect could also occur due to the spatial variability of the material strength, which may influence the propagation of the diagonal crack [57].

As a consequence of the foregoing, the extrapolation of the experimental results to specimens of other dimensions would need to consider the size effect in both the upper and lower shear paths.

5.2. Composite specimens

All the composite specimens displayed similar behaviour when analysing crack patterns. Before reaching V_{exp}, the diagonal cracks at the principal span became horizontal when they reached the flange-web intersection and entered the flange after shortly developing along the flange-web intersection. Immediately after V_{exp}, or shortly before V_{exp} in specimen NWE2, a crack developed along the interface between concretes.

Consequently, the shear strength mechanism observed in these specimens at V_{exp} was the same as that proposed in Fig. 12 for the monolithic specimens. This was supported by similar instrumentation results to those observed in the monolithic specimens: principal span stirrups w4 to w7 were yielded (Fig. 6a), as indicated in Section 4.3; the same tendency of the strain gauges located on top of specimens (see Fig. 11) as observed in the monolithic specimens; similar specimens' crack patterns at V_{exp} as shown in Fig. 9, including the vertical cracks on top of the slab.

Nevertheless, failure was not given by the slab failing in shear, as observed in the monolithic specimens, but by the interface reaching its horizontal shear strength. Consequently, the failure mode in these four specimens was "interface failure" (IF).

As indicated with the monolithic specimens, the maximum shear transmitted through the web below the flange-web intersection was

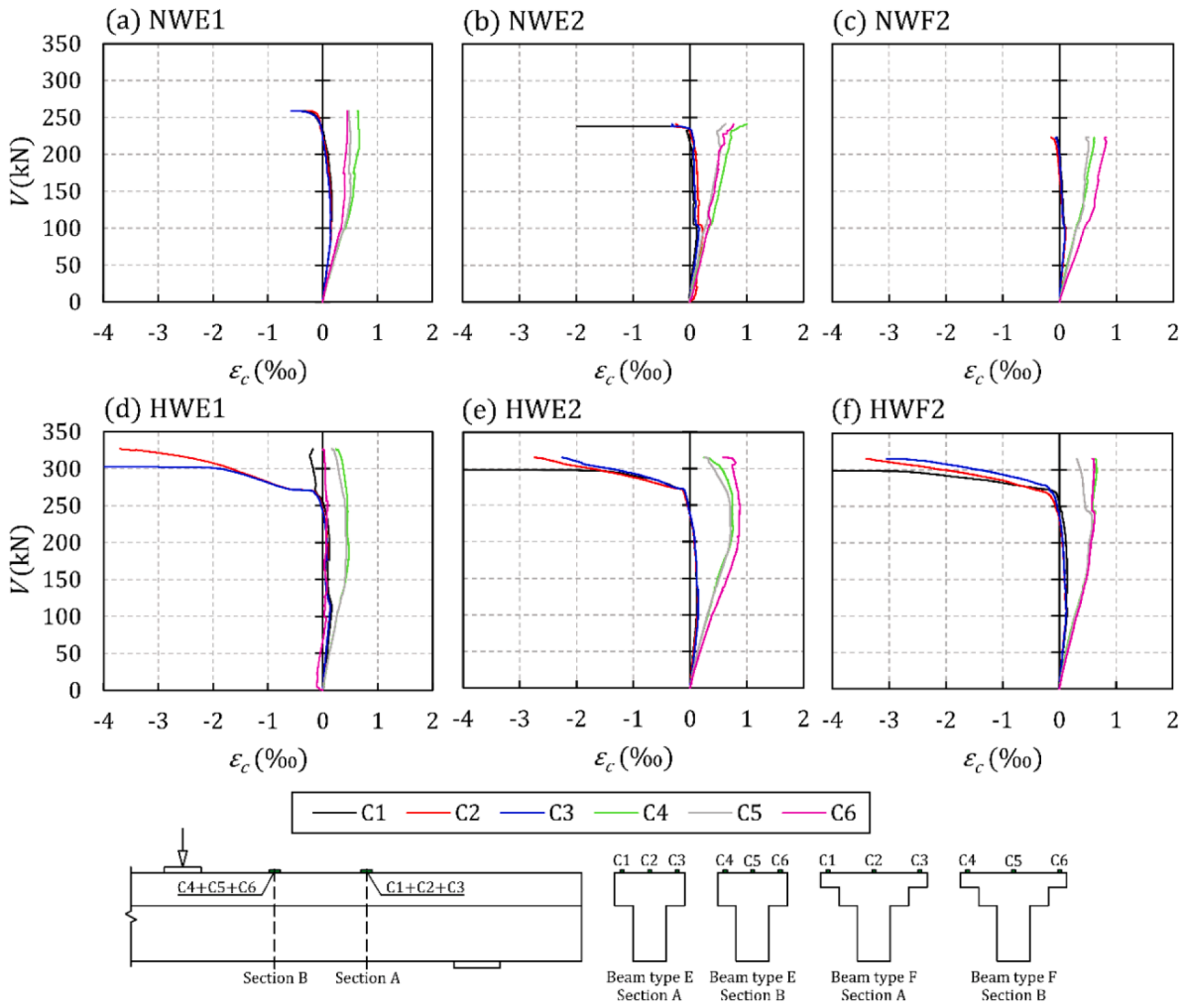

Fig. 11. Measurements of the strain gauges located on top of specimens: (a) specimen NWE1; (b) specimen NWE2; (c) specimen NWF2; (d) specimen HWE1; (e) specimen HWE2; (f) specimen HWF2 (positive ε_c for compression).

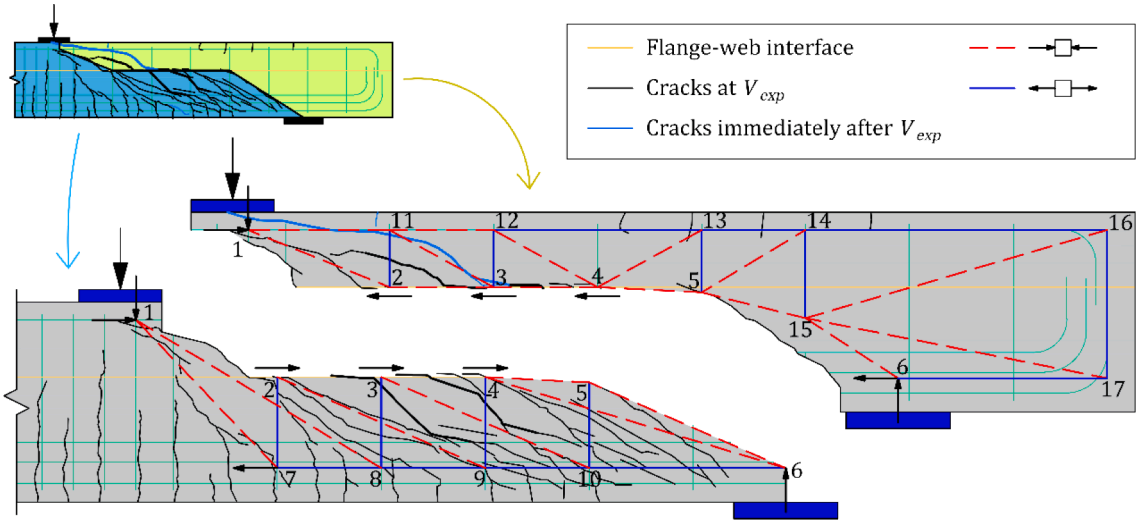

Fig. 12. Authors' proposal about the shear strength mechanism for the monolithic and composite specimens at maximum load (example of specimen HWE1).

considered to be given by the yielding of the stirrups and the inclination of the compression struts. The vertical shear transmitted by the beam head was limited by the interface shear strength.

Other shear strength mechanisms could develop after interface crack formation, such as the dowel action of the web reinforcement at the interface crack and the aggregate interlock at the interface crack. In specimens NWE2 and NWF2, these shear strength mechanisms could maintain a similar shear load to the load that caused IF, as seen on the

smoothly descending branch of their shear-deflection curves in Fig. 8. On the contrary, a marked load drop took place for specimens HWE2 and HWF2 (Fig. 8) because these mechanisms were unable to maintain the load at which the interface crack appeared.

As indicated for monolithic specimens, developing a mechanical model to assess the shear strength of composite specimens will need to reflect the failure mode described, considering the size effect. In addition, to formulate this mechanical model, composite specimens with the characteristics sought in this experimental programme (the interface between concretes modifies the crack pattern) and greater depth would need to be tested. Developing a finite element model calibrated with the experimental results would help formulate the mechanical model. The numerical model for composite specimens has the difficulty of correctly reproducing the interface behaviour. The interface behaviour law could be derived from the use of Digital Image Correlation (DIC) to obtain the normal and tangential stresses at the interface between concretes of the specimens tested.

6. Effect of test parameters on shear strength

6.1. Presence of a cast-in-place slab on top

This section examines the contribution of the cast-in-place slab to shear strength in the T-shaped specimens. The results of three monolithic T-shaped specimens with section type C1 of [34] (Fig. 2), and with the same dimensions and characteristics as the precast T-beam of the composite specimens in this paper (see Fig. 4), were compared to specimen NWE2, which had a cast-in-place slab on top of the precast beam, and specimen NWE1, which had the same cross-sectional shape as NWE2 but without an interface. As specimens C1 had less beam depth, their length and reinforcement were those that gave the same a/d, ρ_l, ρ_w and relative concrete cover (c/h ratio) as the specimens of this experimental programme. The specimens selected for comparison purposes (see Fig. 13) were those with similar concrete compressive strengths.

If the average shear stress of specimen NWE1 is compared to that of series C1, the shear strength decreased on average by 8 % (a simplified calculation was made for this comparison, by considering a shear-effective area of the slab that increases 45° from the cross-section width change, as in [34]). This decrease in the average shear stress of NWE1 was attributed to the size effect. As explained in Section 5.1, the fracture causes a significant deterministic size effect, so that the beam strength decreases as the size of the beam increases.

The average shear stress of specimen NWE2 compared to that of specimens C1 decreased on average by 15 %. The big difference with respect to the value obtained for specimen NWE1 (8 %) indicated that, for specimen NWE2, with two weak planes, not only the size effect decreased shear strength but also the presence of an interface between concretes.

According to the shear strength mechanism explained in Section 5.2 for the composite specimens of this experimental programme (see Fig. 12), the composite specimen's shear strength depended on the shear strength of the interface between concretes. The composite specimen's cast-in-place slab contributed to shear transfer if the interface shear strength of specimen E2 sufficed to reach a higher vertical shear strength than that given by the monolithic precast beam (specimen C1) as the slab provided greater beam head depth. This contribution was limited by the interface shear failure (IF). This was the case of the specimen NWE2.

6.2. Presence of an interface between concretes

To study the influence of the interface between concretes on shear strength, the monolithic specimens with section type E1 (see Fig. 4) were compared to the specimens with the same characteristics, but with an interface between concretes (specimens E2). Fig. 14 shows this comparison for the specimens of series NW and HW of this test programme.

The interface between concretes of specimens E2 reduced shear strength by 7 % and 4 % for series NW and HW, respectively, compared to that of monolithic specimens E1.

The influence of the interface on composite specimens' shear strength can be explained by the shear strength mechanism introduced in Section 5. Accordingly, the interface can affect shear strength in three different ways: firstly, if the interface shear strength is very high, the composite beam (E2 in this test programme) behaves as a monolithic specimen and the specimen fails by SF. Conversely, if the interface shear strength is too low, the slab cannot contribute to resist shear and the composite specimen's shear strength is that of the T-beam without the slab; finally, interface shear strength takes an intermediate value, for which the cast-in-place slab contributes to resist shear until IF.

The last situation occurred in the specimens of this experimental programme. By comparing the shear strengths of specimens C1, E1 and E2 from series NW (Fig. 13 and Fig. 14), the shear strength of specimen E2 was 7 % lower than that of specimen E1, and was 19 % higher than that of specimen C1.

6.3. Slab width

In Fig. 15 the shear strengths of the specimens with section types E2 and F2, which were compounded from a precast T-beam and a cast-in-place slab with two different widths (see Fig. 4), were compared to study the influence of slab width on composite specimens' shear

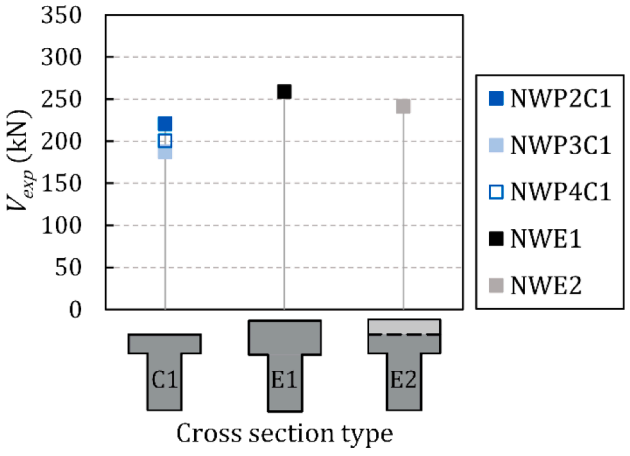

Fig. 13. Comparison between the shear strengths of the specimens with section types C1 [34], E1 and E2 of the NW series.

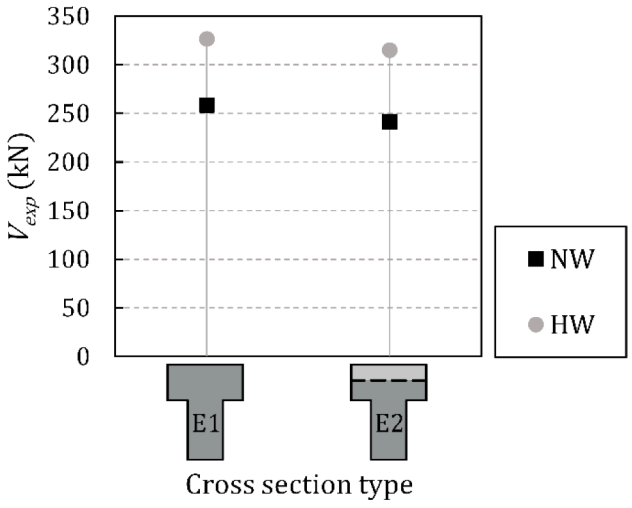

Fig. 14. Comparison between the shear strengths of the specimens with section types E1 and E2.

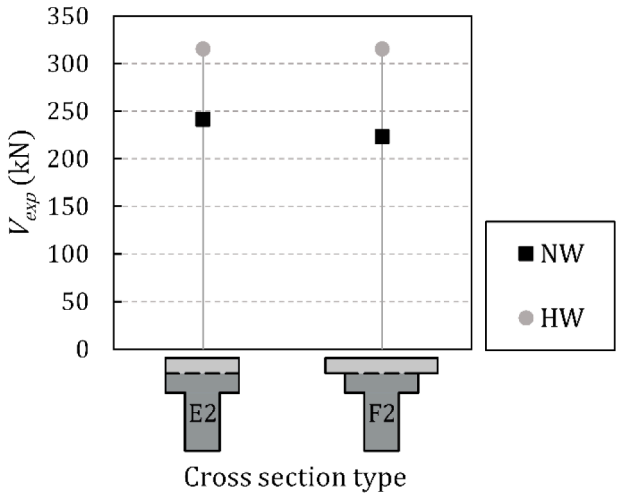

Fig. 15. Comparison between the shear strengths of the specimens with section types E2 and F2.

strength.

Fig. 15 shows that the wider slab of specimen F2 did not increase shear strength compared to specimen E2. In series NW, the shear strength of specimen F2 was 8 % lower than that of specimen E2. In series HW, the wider slab made no difference because the shear strengths of both specimens were the same.

The slight difference in the shear strength of the specimens from series NW could be explained by the position of the neutral axis: in specimen NWF2 with a wider slab, the neutral axis was located higher than in specimen NWE2. Thus for the same shear force, the tangential stress at the interface between concretes was greater in specimen NWF2, so IF occurred with a lower load value. However, this difference in series HW went unnoticed.

Despite the observed results, no general conclusion about the contribution of slab width to shear strength in this specimen type can be drawn. More experimental research should be carried out on composite beams with different dimensions and characteristics to those herein studied.

6.4. Beam and slab concretes' compressive strengths

In this section, the specimens of series NW, with NSC at the precast beam and the slab, are compared to the specimens of series HW, with HSC at the precast beam, to analyse the influence on shear strength of using a better-quality concrete on the precast beam that is commoner in precast concrete plants.

As observed in Fig. 14 and Fig. 15, all the series HW specimens had higher shear strengths than their homologous series NW specimens. Shear strengths were 26 %, 31 % and 41 % higher for specimens E1, E2 and F2, respectively.

In monolithic specimens E1, this increase in the shear strength of series HW could be given by: (i) the higher shear strength of the web below the flange-web intersection as better-quality concrete allowed a lower angle of the compression struts at the web (higher cotθ); (ii) the existence of HSC at the flange, which increased the strength of the flange failing in shear (SF), as shown in [33] and [34].

In the composite specimens, in which the slab concrete had a lower compressive strength than the beam concrete, the shear strength increase of specimens HW could be due to: (i) the higher shear strength of the beam web given by the higher cotθ; (ii) the presence of HSC in part of the composite beam head, which could make the location of the neutral axis higher and, therefore, lower the tangential stresses at the interface and postpone IF, i.e., the IF, which was the failure mode of the composite specimens of this experimental programme, occurred at a higher load than in the specimens made with NSC at both the precast beam and slab.

7. Comparing the test results to existing code provisions

The shear strengths of the test specimens predicted by current codes' shear formulations are analysed in this section. Three shear design procedures for beams with shear reinforcements were considered: formulation of EC2 [29]; the Level III Approximation of MC-10 [31]; the formula (b) of Table 22.5.5.1 of ACI 318-19 [23].

It should be noted that these three formulations neglect flanges' shear strength and, as explained in Section 1, they state that the shear strength of the entire composite specimen can only be considered if the interface is designed to resist the loads that will be transferred across it. Therefore, three shear strength values were calculated in this paper for composite specimens: that which produces IF ($V_{pred,if}$); the shear resistance of the precast beam alone ($V_{pred,pb}$); the shear resistance of the entire composite specimen as if it were a monolithic beam ($V_{pred,mb}$). The predicted shear strength V_{pred} was taken as $V_{pred,mb}$ if the shear force that produced IF $V_{pred,if}$ was higher. If not, V_{pred} was taken as $V_{pred,if}$ if it was higher than the shear strength of the precast beam alone $V_{pred,pb}$, or as $V_{pred,pb}$ if not. Thus $V_{pred} = \min\{V_{pred,mb}; \max\{V_{pred,pb}; V_{pred,if}\}\}$. To calculate $V_{pred,if}$, the interface shear strength was obtained from the formulation of the corresponding code for "smooth" or "as-cast" surfaces with interface reinforcement. $V_{pred,mb}$ was calculated by using the beam concrete compressive strength ($f_{c,b}$) in the EC2 formulation to obtain the maximum cotθ, limited by the crushing of the compression struts at the beam web. In the MC-10 and ACI 318–19 formulations, the weighted average of the compressive strengths of the beam and slab concretes estimated from the area ratio ($f_{c,wa}$) was used. $f_{c,wa}$ has been considered in previous research works [4,11,32–34,40]. It derived from the interpretation of Section 22.5.4 of ACI 318–19 for shear in composite concrete members, and proved to give accurate results and on the safety side when assessing composite elements. The results are presented in Table 4.

The tested average values of the material properties were used for all the formulations. The partial safety factors for concrete and steel material properties were taken as 1.0.

The results presented in Table 4 show that the current codes' formulations underestimated the shear strength of the monolithic and composite T-shaped specimens of this test programme, possible for two reasons: neglecting flanges' shear strength in the T-beams and underestimating the interface shear strength in the composite specimens as these specimens' predicted shear strength was always that of the precast T-beam alone ($V_{pred,pb}$).

According to Table 4, EC2 gave the best approximation for the specimens made of NSC (series NW) of the three considered codes. However for the specimens made of HSC, EC2 offered a much more conservative shear strength estimation than the other two codes because the EC2 shear formulation does not depend on concrete compressive strength for the specimens of this experimental programme. On the contrary, the MC-10 and ACI 318-19 formulations, which depend on concrete compressive strength, had similar V_{exp}/V_{pred} ratios of specimens HW to those of specimens NW with the same cross-sectional shape.

Table 4 shows the mean value and the CV of V_{exp}/V_{pred} for the six specimens of this test programme. The three considered formulations obtained a similar mean value. However, the CV of EC2 was very high (16.17 %) compared to that of MC-10 (9.73 %) and ACI 318-19 (5.79 %). This indicates that ACI 318-19 better considered the influence of beam concrete compressive strength on the shear strength of the specimens of this test programme. Nevertheless, the high V_{exp}/V_{pred} mean values obtained with these three shear strength formulations revealed that they did not well capture the influence of the existence of both flanges and a cast-in-place slab. Thus to improve the current design shear formulations' accuracy, the effect of flanges should be considered and the interface shear strength should be better estimated.

Table 4
The V_{exp}/V_{pred} ratios for the test specimens assessed with current codes' formulations.

Code formulation	NWE1	HWE1	NWE2	HWE2	NWF2	HWF2	Mean	CV (%)
EC2 [29]	1.33	1.68	1.55	2.03	1.44	2.03	1.68	16.17
MC-10 LIII [31]	1.41	1.52	1.63	1.82	1.50	1.82	1.62	9.73
ACI 318-19 (b) [23]	1.53	1.47	1.72	1.69	1.59	1.69	1.61	5.79

8. Summary and conclusions

This paper presents the results of six reinforced concrete T-shaped specimens subjected to shear forces, with shear reinforcement and heavily longitudinally reinforced, which were experimentally tested to study the cast-in-place slab contribution to shear strength in concrete composite beams. By comparing different cross-section types and concrete qualities, the following points that influence shear strength were studied: the existence of a cast-in-place slab; the presence of an interface between concretes; cast-in-place slab width; the compressive strength of the beam and slab concretes. The observed shear strength mechanisms were analysed. Finally, the experimental shear strength was compared to that predicted by current design codes. The main findings of this study are:

1. In the monolithic T-beams, the cross-section width change is a weakness plane that deviates the diagonal shear cracks along it and divides the shear transmission into two load paths: one through the beam web below the cross-section width change and one through the beam head or flange. Failure occurs when the upper path, that at the flange, reaches its shear strength.
2. In the T-beams with a cast-in-place slab on top (composite beams), the interface between the T-beam and slab may crack at failure. Thus failure occurs when the interface shear stress exceeds the interface shear strength.
3. The composite specimen's shear strength takes an intermediate value between the shear strengths of the T-shaped specimen with no cast-in-place slab and the monolithic T-shaped specimen with the same depth as the composite specimen. The higher or lower strength is given by the interface shear strength.
4. For the specimens of this test programme, a wider cast-in-place slab did not increase the shear strength of the specimens. The 8 % decrease observed in specimens NW can be explained by the rise in the neutral axis, which increases interface shear stresses and leads to premature interface failure.
5. The use of HSC on the precast beam in composite specimens increased shear strength by 36 % on average because it allows a greater inclination of the compression struts at the beam web and postpones IF by reducing interface shear stresses since the neutral axis is higher.
6. The shear formulations for beams with web reinforcements of EC2, MC-10 Level III and ACI 318-19 formula (b) predicted very conservative shear strengths for the specimens tested in this experimental programme (experimental-to-predicted shear strength ratios of 1.68, 1.62 and 1.61, respectively, on average for all the specimens) because the shear strength of flanges is neglected and interface shear strength is underestimated. ACI 318-19 offered the most accurate results with a low CV (5.79 %), so this formulation best captured the effect of concrete compressive strength on shear strength.

The present paper provides experimental results about the contribution of the cast-in-place slab to shear strength in concrete composite beams, and analyses the shear strength mechanisms that these specimens develop. It sheds light on future shear formulation development for composite concrete elements. However, more experimental tests should be conducted in composite beams with an interface between concretes that modifies the shear strength mechanisms, for example, in specimens with different beam depths to deepen the size effect, different a/d ratios to analyse the effect of the arching action, or with prestressed reinforcement to understand better the shear behaviour of these structural elements, which are so common in current constructions. The development of a numerical model that correctly represents the interface behaviour law and the formulation of a mechanical model for the shear strength assessment of concrete composite beams, derived from the analysis of the existent and the additional test results, are two main future research lines on this topic.

Declaration of Competing Interest

The authors declare that they have no known competing financial interests or personal relationships that could have appeared to influence the work reported in this paper.

Data availability

Data will be made available on request.

Acknowledgements

Ministerio de Ciencia e Innovación (MCIN) and *Agencia Estatal de Investigación* (AEI) supported the present research work through grants BIA2015-64672-C4-4-R and RTI2018-099091-B-C21-AR, both funded by MCIN/AEI/ 10.13039/501100011033 and by "ERDF A way of making Europe". Author Lisbel Rueda-García was supported by grant BES-2016-078010 funded by MCIN/AEI/ 10.13039/501100011033 and by "ESF Investing in your future". The project was also carried out with the support of the Regional Government of Valencia through Project AICO/2018/250. The open access charge was funded by CRUE-Universitat Politècnica de València. This research work was undertaken at the Concrete Science and Technology University Institute (ICITECH) of the Universitat Politècnica de València (UPV; Spain) with concrete supplied by Caplansa.

References

[1] Comité technique 4.3 - Ponts routiers Technical Committee 4.3 - Road Bridges. Estimation of load carrying capacity of bridges based on damage and deficiency. PIARC World Road Association: 2016.
[2] Ayensa A, Oller E, Beltrán B, Ibarz E, Marí A, Gracia L. Influence of the flanges width and thickness on the shear strength of reinforced concrete beams with T-shaped cross section. Eng Struct 2019;188:506–18. https://doi.org/10.1016/j.engstruct.2019.03.057.
[3] Martinelli E. A general numerical model for simulating the long-term response of two-layer composite systems in partial interaction. Compos Struct 2021;257:112929. https://doi.org/10.1016/j.compstruct.2020.112929.
[4] Kim C-G, Park H-G, Hong G-H, Kang S-M. Shear strength of composite beams with dual concrete strengths. ACI Struct J 2016;113:263–74. https://doi.org/10.14359/51688061.
[5] Soltani M, Ross BE. Database evaluation of interface shear transfer in reinforced concrete members. ACI Mater J 2017;114(383–94). 10.14359/51689249.
[6] Mast RF. Auxiliary reinforcement in concrete connections. J Struct Div ASCE 1968;94:1485–504.
[7] Birkeland PW, Birkeland HW. Connections in precast concrete construction. ACI J Proc 1966;63:345–68.
[8] Mattock AH, Hawkins NM. Shear transfer in reinforced concrete—Recent research. PCI J 1972;17(55–75). https://doi.org/10.15554/pcij.03011972.55.75.
[9] Loov RE, Patnaik AK. Horizontal shear strength of composite concrete beams with a rough interface. PCI J 1994;39:48–69. https://doi.org/10.15554/pcij.01011994.48.69.
[10] Kahn LF, Slapkus A. Interface shear in high strength composite T-beams. PCI J 2004;49:102–10. https://doi.org/10.15554/pcij.07012004.102.110.

[11] Kim C-G, Park H-G, Hong G-H, Kang S-M, Lee H. Shear strength of concrete composite beams with shear reinforcements. ACI Struct J 2017;114:827–37. https://doi.org/10.14359/51689441.
[12] Avendaño AR, Bayrak O. Shear strength and behaviour of prestressed concrete beams. Technical Report: IAC-88-5DD1A003-3, Texas Department of Transportation: 2008.
[13] Nagle TJ, Kuchma DA. Nontraditional limitations on the shear capacity of prestressed concrete Girders. University of Illinois at Urbana-Champaign 2007.
[14] American Association of State Highway and Transportation Officials (AASHTO). AASHTO LRFD Bridge design specifications. 4th edition. Washington, DC: AASHTO; 2007.
[15] Ross BE, Hamilton HR, Consolazio GR. Experimental study of end region detailing and shear behavior of concrete i-girders. J Bridg Eng 2015;20. https://doi.org/10.1061/(ASCE)BE.1943-5592.0000676.
[16] Ruiz MF, Muttoni A. Shear strength of thin-webbed post tensioned beams. ACI Struct J 2009;106.
[17] Tawfiq K. Cracking and shear capacity of high strength concrete girders. 1996.
[18] Hamilton III HR, Llanos G, Ross BE. Shear performance of existing prestressed concrete bridge girders. 2009.
[19] Runzell B, Shield C, Shear FC. Capacity of Prestressed Concrete Beams 2007.
[20] Shahawy MA, Batchelor BdeV. Shear Behavior of full-scale prestressed concrete girders: Comparison between AASHTO specifications and LRFD Code. PCI J 1996; 41:48–62. https://doi.org/10.15554/pcij.05011996.48.62.
[21] Ross BE, Ansley MH, Hamilton III HR. Load testing of 30-year-old AASHTO Type III highway bridge girders. PCI J 2011;56.
[22] Raymond KK, Bruce RN, Roller JJ. Shear Behavior of HPC Bulb-Tee Girders. Seventh Int Symp Util High-Strength / High-Performance 2005;3:705–22.
[23] ACI Committee 318. 318-19 Building Code Requirements for Structural Concrete and Commentary. American Concrete Institute; 2019. Doi: 10.14359/51716937.
[24] Halicka A. Influence new-to-old concrete interface qualities on the behaviour of support zones of composite concrete beams. Constr Build Mater 2011:4072–8. https://doi.org/10.1016/j.conbuildmat.2011.04.045.
[25] Rueda-García L, Bonet JL, Miguel Sosa PF, Fernández Prada MÁ. Safety assessment of shear strength current formulations for composite concrete beams without web reinforcement. In: Fédération Internationale du Béton (fib), editor. Proc. 2021 fib Symp. Concr. Struct. New Trends Eco-Efficiency Perform., Lisbon: 2021, p. 2305–14.
[26] Halicka A, Jabłoński Ł. Shear failure mechanism of composite concrete T-shaped beams. Proc Inst Civ Eng - Struct Build 2016;169:67–75. https://doi.org/10.1680/stbu.14.00127.
[27] Kim C-G, Park H-G, Hong G-H, Lee H, Suh J-I. Shear Strength of RC-composite beams with prestressed concrete and non-prestressed concrete. ACI Struct J 2018; 115. https://doi.org/10.14359/51702224.
[28] Kim C-G, Park H-G, Hong G-H, Kang S-M. Shear strength of composite beams with steel fiber-reinforced concrete. ACI Struct J 2019;116. https://doi.org/10.14359/51716812.
[29] CEN. EN 1992-1-1:2013. Eurocode 2: Design of concrete structures - Part 1-1: General rules and rules for buildings. 2004.
[30] PCI Bridge Design Manual, 3rd edition. Precast/Prestressed Concrete Institute; 2014. 10.15554/MNL-133-14.
[31] Fédération International du Béton (fib). Model Code 2010. Ernst & Sohn; 2012.
[32] Rueda-García L, Bonet Senach JL, Miguel Sosa PF, Fernández Prada MÁ. Experimental analysis of the shear strength of composite concrete beams without web reinforcement. Eng Struct 2021;229:111664. https://doi.org/10.1016/j.engstruct.2020.111664.
[33] Rueda-García L, Bonet Senach JL, Miguel Sosa PF, Fernández Prada MÁ. Analysis of the shear strength mechanism of slender precast concrete beams with cast-in-place slab and web reinforcement. Eng Struct 2021;246:113043. https://doi.org/10.1016/j.engstruct.2021.113043.
[34] Rueda-García L, Bonet Senach JL, Miguel Sosa PF, Fernández Prada MÁ. Experimental study on the shear strength of reinforced concrete composite T-shaped beams with web reinforcement. Eng Struct 2022;255:113921. https://doi.org/10.1016/j.engstruct.2022.113921.
[35] Placas A. Shear failure of reinforced concrete beams. Faculty of Engineering of the University of London, Imperial College of Science and Technology; 1969.
[36] Ribas González CR, Fernández RM. Influence of flanges on the shear-carrying capacity of reinforced concrete beams without web reinforcement. Struct Concr 2017. https://doi.org/10.1002/suco.201600172.
[37] Fernández Ruiz M, Muttoni A, Sagaseta J. Shear strength of concrete members without transverse reinforcement: A mechanical approach to consistently account for size and strain effects. Eng Struct 2015;99:360–72. https://doi.org/10.1016/j.engstruct.2015.05.007.
[38] Kani MW, Mark W. Huggins, Rudi R. Wittkopp. Kani on shear in reinforced concrete. Toronto: University of Toronto, Dept. of Civil Engineering; 1979.
[39] Cladera A. Shear design of reinforced high-strength concrete beams. Doctoral thesis. Universitat Politècnica de Catalunya. http://hdl.handle.net/10803/6155.
[40] Rueda-García L, Bonet Senach JL, Miguel Sosa PF. Experimental study of concrete composite beams subjected to shear. In: Proc. fib Symp. 2019 Concr. - Innov. Mater. Des. Struct., 2019, p. 1779–86.
[41] UNE-EN 12390-3:2020. Testing hardened concrete - Part 3: Compressive strength of test specimens. 2020.
[42] UNE-EN 12390-6:2010. Testing hardened concrete - Part 6: Tensile splitting strength of test specimens. 2010.
[43] UNE-EN 12390-13:2014. Testing hardened concrete - Part 13: Determination of secant modulus of elasticity in compression. 2014.
[44] Comisión Permanente del Hormigón. EHE-2008. Madrid: Instrucción de Hormigón Estructural. Ministerio de Fomento; 2008.
[45] UNE-EN ISO 6892-1:2017. Metallic materials - Tensile testing - Part 1: Method of test at room temperature. 2017.
[46] Miguel-Tortola L, Miguel PF, Pallarés L. Strength of pile caps under eccentric loads: Experimental study and review of code provisions. Eng Struct 2019;182:251–67. https://doi.org/10.1016/j.engstruct.2018.12.064.
[47] Monserrat López A, Miguel Sosa PF, Bonet Senach JL, Fernández Prada MÁ. Influence of the plastic hinge rotations on shear strength in continuous reinforced concrete beams with shear reinforcement. Eng Struct 2020;207:110242. https://doi.org/10.1016/j.engstruct.2020.110242.
[48] Palaskas MN, Attiogbe EK, Darwin D. Shear strength of lightly reinforced T-beams. J Am Concr Inst 1981;78:447–55.
[49] Pansuk W, Sato Y. Shear mechanism of reinforced concrete T-Beams with stirrups. J Adv Concr Technol 2007;5. https://doi.org/10.3151/jact.5.395.
[50] Giaccio C, Al-Mahaidi R, Taplin G. Experimental study on the effect of flange geometry on the shear strength of reinforced concrete T-beams subjected to concentrated loads. Can. J Civ Eng 2002;29. https://doi.org/10.1139/l02-099.
[51] Leonhardt F, Walther R. Schubversuche an einfeldrigen Stahlbetonbalken mit und ohne Schubbewehrung zur Ermittlung der Schubtragfähigkeit und der oberen Schubspannungsgrenze, Heft 151. Berlin: Ernst & Sohn; 1962.
[52] Yu Q, Bažant ZP. Can stirrups suppress size effect on shear strength of RC beams? J Struct Eng 2011;137:607–17. https://doi.org/10.1061/(ASCE)ST.1943-541X.0000295.
[53] Bažant ZP, Yu Q. Designing against size effect on shear strength of reinforced concrete beams without stirrups: I Formulation. J Struct Eng 2005;131:1877–85. https://doi.org/10.1061/(ASCE)0733-9445(2005)131:12(1877).
[54] Bažant ZP, Yu Q. Designing against size effect on shear strength of reinforced concrete beams without stirrups: II. Verification and Calibration. J Struct Eng 2005;131:1886–97. https://doi.org/10.1061/(ASCE)0733-9445(2005)131:12(1886).
[55] Bažant ZP, Yu Q, Gerstle WH, Hanson JH, Ju JW. Justification of ACI 446 proposal for updating ACI code provisions for shear design of reinforced concrete beams. ACI Struct J 2007;104:601–10.
[56] ACI Committee 446 Fracture Mechanics. ACI PRC-446.1-91: Fracture Mechanics of Concrete: Concepts, Models and Determination of Material Properties (Reapproved 1999). 2002.
[57] Hunter MD, Ferche AC, Vecchio FJ. Influence of spatial variability of concrete in large shear- critical structures. ACI Struct J 2021;118. https://doi.org/10.14359/51728194.